Journal of Alloys and Compounds 503 (2010) 242–247

Contents lists available at ScienceDirect

Journal of Alloys and Compounds

journal homepage: www.elsevier.com/locate/jallcom

Role of molybdenum ions on physical, optical, electrical and vibrational studies in Er^{3+} co-doped TeO_2–ZrO_2–$PbCl_2$ glasses

Shaaban M. Salem*

Department of Physics, Faculty of Science, Al Azhar University, Nasr City 11884, Cairo, Egypt

ARTICLE INFO

Article history:
Received 7 October 2009
Accepted 3 May 2010
Available online 9 May 2010

Keywords:
Tellurite–lead–zirconium–molybdenum–rare earth-glasses
Raman
Structure
Electrical and optical properties

ABSTRACT

$(75-x)TeO_2$–$15PbCl_2$–$xMoO_3$–$10ZrO_2$ doped with 5 mol% Er_2O_3, where $x = 2.5$, 5, 7.5 and 10 mol%, glasses were investigated by Raman spectroscopy, dc conductivity, optical transmittance spectra and density were measured. Mo═O bonds are present in the entire glass composition. The glasses contain TeO_4 trigonal bipyramids, TeO_{3+1} polyhedra and MoO_6 octahedra as basic structural units. Glasses having low MoO_3 content contain MoO_6 octahedra having two Mo═O bonds. As MoO_3 content increases, the fraction of Mo═O bonds to Mo^{6+} decreases. The dc conductivity increases with increase in MoO_3 content, and the activation energy decreases with increase in MoO_3 content. The optical band gap (E_{opt}) and Urbach energy (E_r) were determined from the optical transmittance spectra of the polished samples recorded in the spectral range from 190 to 1100 nm at room temperature (RT). Variation in these optical parameters has also been associated with the structural changes occurring in these glasses with increase in MoO_3 content, and the present glasses behave as indirect gap semiconductors.

© 2010 Elsevier B.V. All rights reserved.

1. Introduction

Study on tellurite based glasses, has been the subject of high interest due to their potential applications such as IR domes which enlarges the transmission infrared spectra range up to 6 μm, high refractive index, high phonon energy, and an excellent non-linear behavior [1–9]. These properties, due to the high polarizability of Te^{4+}-ions (with a solitary electron pair $5s^2$), can be even more enhanced by means of the incorporation of other heavy metals oxides that can be easily polarized (e.g. MoO_3, PbO, ZrO_2) [6]. Apart from these special optical properties, other advantages of such glasses are their good thermal and chemical stability, low tendency to crystallization and their ability to host rare earth ions. Glasses based on mixed oxide–halide systems combine the good optical properties of halide glasses (a broad range of optical transmittance and low optical losses) with the better chemical and thermal stability of oxide glasses [10]. It is reported that oxide glasses are more appropriate for practical applications due to their high chemical durability and thermal stability [11–13]. Many investigations have focused on oxyhalide tellurite glasses. For example, Raman and FTIR spectra were used to analyze the effect of $ZnCl_2$ on the structure, spectral properties and the nature of the OH^- groups in the glass system [TeO_2–ZnO–$ZnCl_2$] [14]. Optical absorption and photoluminescence properties of Eu^{3+}-doped (TeO_2–ZnF_2–PbO) glasses have been studied and different possible laser emission transitions were discussed [15]. Frequency up-conversion of near infrared radiation NIR to visible light in RE^{3+} doped-glasses has received a great deal of interest for possible wide range of applications. For example, it has been found that the addition of $PbCl_2$ to the glass matrix of the system (GeO_2–BaO–ZnO–PbO–Er_2O_3) results in a lowering of the maximum phonon energy which makes the glass better candidate for up-conversion luminescence applications [10]. Electronic conduction in this type of materials is predicted due to polaron hopping where as the ionic conduction is expected due to the diffusion of alkali ions or any other dopant ions [16,17]. In the recent years an enormous amount of research is being carried out on several physical properties and the chemical durability of tellurite glasses by introducing a number of glass formers and modifiers such asV_2O_5, Cr_2O_3, Fe_2O_3, Al_2O_3, MoO_3, Sb_2O_3, etc. [16–18]. Among various transition metal ions, molybdenum ions are expected to have profound influence on the optical and electrochemical properties of lead tellurite glasses, in view of the fact that the oxide of molybdenum participate in the glass network with different structural units like MoO_4 (T_d) and MoO_6 (O_h) of Mo^{6+} ions and Mo^{5+} O_3^- (O_h) of Mo^{5+} ions [18].

The aim of the present work is to investigate the effect of MoO_3 content on the structure, electrical and optical properties of oxychloride tellurite TeO_2–MoO_3–ZrO_2–$PbCl_2$ doped with Er^{3+} glasses obtained and to determine some of their properties. The glass samples were investigated using X-ray diffraction, density, FT-Raman, dc conductivity and optical transmittance spectra.

* Tel.: +2038952044.
E-mail address: shaabansalem@gmail.com.

0925-8388/$ – see front matter © 2010 Elsevier B.V. All rights reserved.
doi:10.1016/j.jallcom.2010.05.009

Table 1
Chemical composition and physical properties of the $(75-x)TeO_2$–$15PbCl_2$–$xMoO_3$–$10ZrO_2$ doped with 5 mol% Er_2O_3, where x = 2.5, 5, 7.5 and 10 mol% glass system.

Glass no.	Composition (mol%)					d (g cm^{-3})	V_m (cm^3/mol)	$N \times 10^{21}$ (cm^{-3})	R (Å)	W (eV)
	TeO_2	$PbCl_2$	MoO_3	ZrO_2	Er_2O_3					
1	72.5	15	2.5	10	5	5.632	31.03	0.88	10.4	0.92
2	70	15	5	10	5	5.583	31.23	1.75	8.29	0.89
3	67.5	15	7.5	10	5	5.397	32.23	2.54	7.33	0.88
4	65	15	10	10	5	5.177	33.53	3.25	6.75	0.86

2. Experimental

Glasses of the composition $(75-x)TeO_2$–$15PbCl_2$–$xMoO_3$–$10ZrO_2$ doped with 5 mol% Er_2O_3, where x = 2.5, 5, 7.5 and 10 mol%, have been prepared by the conventional melting and quenching method. The mixture of these chemicals taken in porcelain crucibles and then melted at 900 °C by using electrical furnace for 30 min to ensure homogeneous mixture. The clear liquid (free of bubbles) was quickly cast in a copper mould kept at room temperature and pressed with another copper disc maintained at the same temperature, the obtained glass samples were transparent. Bulk samples of ~2 cm diameter and ~0.5 mm thickness were obtained. X-ray powder diffraction XRD measurements have been carried out on (Shimadzu XD-DI, X-ray Diffractometer VG 207RII and Cu Kα = 1.54056 Å) for grounded powder of the as-quenched samples as a necessary technique for proving the amorphous nature of the samples. The density of the samples measured at room temperature was measured by Archimedes principle using carbon tetrachloride as an immersion liquid. The molar volume (V_m), the concentration of molybdenum ions N and the intermediate distance between molybdenum ions R were estimated. The dc electrical conductivity measured by means of two-probe method, which appropriate for high resistance materials. Silver painted electrodes were pasted on the polished surface of the samples then situated between two polished and cleaned copper electrodes. The current is monitored by means of an electrometer [model: 425A HP], milivoltmeter for measuring the temperature over temperature range (300–650 K) with constant voltage source 18 V and a home-made furnace. The optical transmittance spectra of the present glasses were recorded at room temperature in the wavelength range 190–1100 nm using Jasco V-570 Spectrophotometer. The FT-Raman spectra were measured for the as-casting samples using Bruker FT-Raman spectrometer of type RFS 100/S, which is attached to Bruker-IFS 66/s spectrometer. The RFS 100/S version provides flexible sample handling and optimum FT-Raman performance. This system is equipped with a broad-range Quartz beam splitter; Bruker's patented frictionless interferometer with its rock solid alignment provides high sensitivity and stability. The diode-pumped, air-cooled Nd–YAG laser source with maximum laser power of 1500 mW is controlled completely through software. Raman spectra of the as-casting bulk glass samples of have been measured with a resolution of 2 cm^{-1} using 1064 nm laser line with a power of 100 mW over the whole spectral range.

3. Results and discussion

3.1. Density and molar volume

The values of the density ρ for all glass samples are given in Table 1 with probable error of ±0.001. The molar volume V_m of the glass samples was calculated using the molecular weight of the glass samples M and density ρ with the following relation:

$$V_m = \frac{M}{\rho} \quad (1)$$

The concentration of molybdenum ions, N(cm^{-3}), was estimated using $N = \rho p N_A / A_w \times 100$, where ρ is the density of the sample, p is the weight percentage of atoms, N_A is the Avogadro's constant and A_w is the molecular weight of molybdenum ions, and the enter atomic distance between molybdenum ions $R = (1/N)^{1/3}$.

The variations of density and molar volume with the concentration of MoO_3 mol% are shown in Fig. 1. It is evident from Fig. 1 and Table 1 that the density of the present glass system decreases with increase in MoO_3 content, while the molar volume increase with increase in MoO_3 content. The ionic concentration of molybdenum ions and inter-ionic distance have been calculated and included in Table 1. The decrease in the density values as the MoO_3 content increase can be attributed to the MoO_3 have molecular mass less than TeO_2. On the other hand, an increase in bond length, cross-link density and closeness of packing, are responsible for decrease

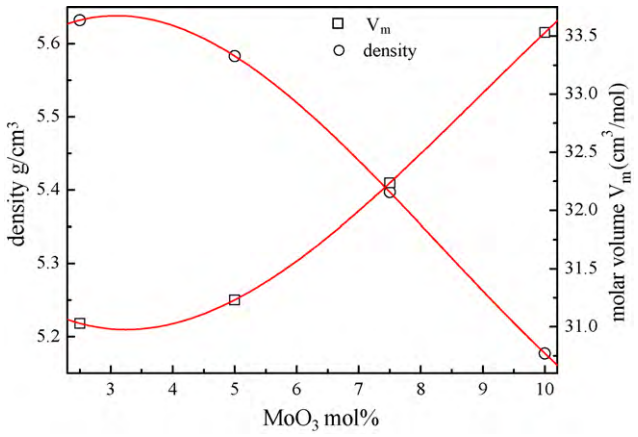

Fig. 1. The density d and molar volume V_m as a function of MoO_3 content for the $(75-x)TeO_2$–$15PbCl_2$–$xMoO_3$–$10ZrO_2$ doped with 5 mol% Er_2O_3, where x = 2.5, 5, 7.5 and 10 mol% glass system.

of density and increase of molar volume. Such an observation indicates that there is an increasing presence of molybdenum ions in Mo^{6+} state that take part in network forming positions with MoO_4^{2-} tetrahedral structural units with increase in the concentration of MoO_3 and cause a reduction of cross-link density and weakening of the mean bond strength in the glass network probably due to the increasing concentration of octahedrally sited molybdenum which in good agreement with Raman results [19].

3.2. Raman spectra

Fig. 2 shows the changes of Raman scattering spectra monitored the $(75-x)TeO_2$–$15PbCl_2$–$xMoO_3$–$10ZrO_2$ doped with 5 mol% Er_2O_3, where x = 2.5, 5, 7.5 and 10 mol%, glass system in the range of (80–1100) cm^{-1}. Strong bands are distinguished at ~150, 284,

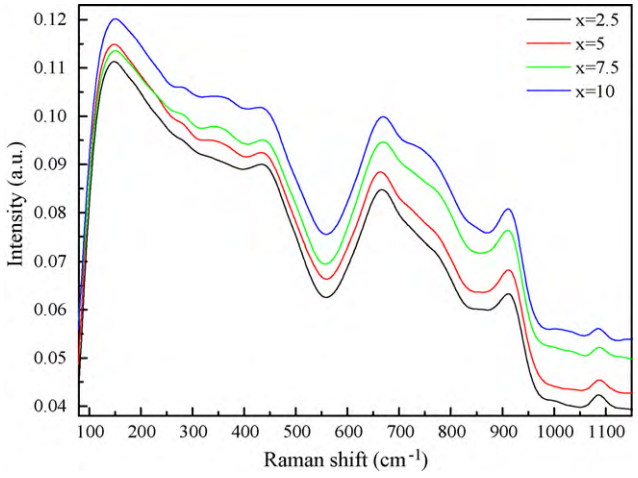

Fig. 2. Raman spectra for the $(75-x)TeO_2$–$15PbCl_2$–$xMoO_3$–$10ZrO_2$ doped with 5 mol% Er_2O_3, where x = 2.5, 5, 7.5 and 10 mol% glasses.

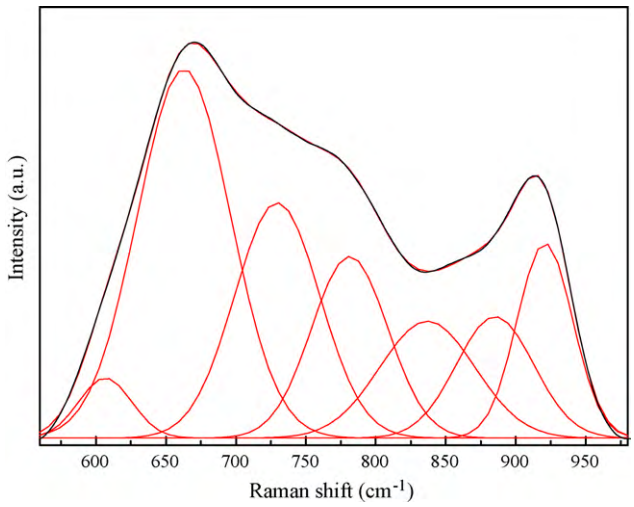

Fig. 3. Deconvoluted Raman spectra in the frequency range (80–1150) cm^{-1} for the sample containing 2.5 mol% MoO_3.

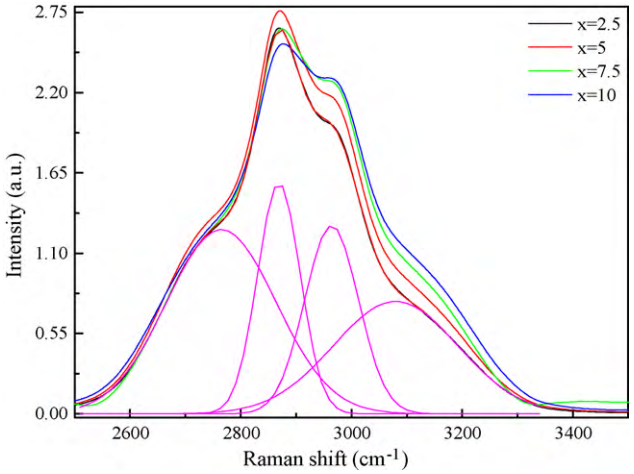

Fig. 4. Raman spectra in the high frequency range (2500–3400) cm^{-1} for the $(75-x)TeO_2$–$15PbCl_2$–$xMoO_3$–$10ZrO_2$ doped with 5 mol% Er_2O_3, where x = 2.5, 5, 7.5 and 10 mol% glasses.

362, 450, 667, 720, 775, 855 and 912 cm^{-1}. The Raman band at 150 cm^{-1} is corresponding to the peak at 150 cm^{-1} of crystalline TeO_2, it is assigned as a boson peak associated to light scattering due to acoustic-like vibrations of the disordered structure. It has been considered characteristic of glasses (observed for most inorganic glasses including tellurites), some liquids and colloids and were assigned to rocking and localized or acoustic Raman modes [20,21]. Boson peak refers to an excess contribution to the usual Debye density of states (DOS) at low frequencies and is considered as a characteristic anomaly of disordered materials [22]. Several models associate this band to some structural length by $R = V_t/\omega_{max}$, where ω_{max} is the frequency of the maximum of the boson peak and V_t is the velocity of the transverse sound wave propagating through the sample [23]. The band at 450 cm^{-1} is usually ascribed to bending vibrations of (Te–O–Te) linkages [3,6–9], which are formed by vertex sharing of TeO_4, TeO_{3+1} and TeO_3 polyhedra, with increasing MoO_3 content, this band shifts towards lower frequency and its relative intensity increases as shown in Fig. 2. The presence and relative intensity of these two bands is a measure of the network connectivity in TeO_2-based glasses [24] (Fig. 3).

The band at 667 cm^{-1} is assigned to the axial symmetric stretching vibration modes $(Te_{ax}–O)_s$ of the TeO_4 trigonal bipyramids tbps with bridging oxygen BO atoms [25,26]. As found in the literature, this band has been assigned to coupled symmetric vibrations along Te–O–Te axes in $TeO_{3+\delta}/TeO_4$, and TeO_4/TeO_3 pairs and was suggested to be a relative measure of the connectivity between $TeO_{3+\delta}$, TeO_4, and TeO_3 species [24]. It is corresponding to the known [27] strong Raman band of crystalline α-TeO_2 at 646 cm^{-1}. The Raman bands at ~720 and at ~775 cm^{-1} are due to the formation of TeO_{3+1} and/or TeO_3 pyramids associated with NBO in the glassy sample [3–5,12,28]. These two bands are assigned to stretching mode contributions from TeO_4 trigonal bipyramids tbps, $TeO_{3+\delta}$ polyhedra and TeO_3 tps [24]. TeO_4 tbps are connected through $(Te_{eq}–O_{ax}–Te)$ bonds forming a three-dimensional network. Earlier neutron scattering and Raman spectral studies on TeO_2 glasses containing different modifiers have reported that the basic building blocks of TeO_2-based glasses are the tbps [29]. Based on many previous spectral studies, it has been concluded that these TeO_4 tbps convert to TeO_{3+1} polyhedra and/or TeO_3 trigonal pyramids tps depending on the amount of the added modifier. The bands at 840 and 912 cm^{-1} are assigned to the stretching vibrations of (Mo=O) bonds of the deformed MoO_6 octahedra and to the vibrations of (Mo–O–Mo) bridging bonds, respectively [28]. The bands at ~667, 720 and 775 cm^{-1} of the basic glass shift slightly to lower energies as MoO_3 increases that are can be attributed to the addition of the MoO_3 ions in the glass network leads to reduction of the phonon vibration energies.

The Raman spectra of Fig. 2 are fitted to seven Gaussian peaks at 607, 662, 729, 781, 840, 885 and 929 cm^{-1}, it is evident from Fig. 2, that the addition of MoO_3 the area under the peak at 729 cm^{-1} increases while the area under the peak at 670 cm^{-1} is decreasing. This behavior may suggest a gradual change of TeO_4 tbps to TeO_{3+1} and/or TeO_3 [24]. Therefore it could be concluded that the successive introduction of MoO_3 in the present glasses leads to the progressive formation of distorted TeO_{3+1} units followed by the creation of trigonal TeO_3 pyramids (tps) associated with non-bridging oxygen atoms (NBO) [28]. As is known, the increase in the modifier concentration in tellurite glasses leads to the progressive formation of distorted TeO_{3+1} units followed by the creation of regular trigonal TeO_3 pyramids (tps) associated with non-bridging oxygen atoms (NBO) [28,30]. The area under the peak of the two bands 885 and 920 cm^{-1} increases as the MoO_3 content increase. This may suggest that addition of MoO_3 leads to more formation of Mo–O–Mo bridging bonds in favor of the Mo=O doubly degenerate stretching vibrations of the deformed MoO_6 octahedra [28] (Fig. 3).

Raman spectra in the high frequency range (2500–3400) cm^{-1} is shown in Fig. 4 The Raman bands at 2765, 2870, 2980 and 3085 cm^{-1} are assigned to vibrations of the OH^- groups [31]. The fundamental OH^- band was found to peak at ~2980 cm^{-1} (3.356 μm). The broadening of the OH^- band is related to the amorphous nature of the glass and is believed that NBO contribute to the hydrogen bonding in the glassy matrix [31]. It has been deconvoluted to 4 bands at 2764, 2869, 2964, 3080 cm^{-1}. The OH^- vibration modes have been detected before in many tellurite glasses in the range (2500–3500 cm^{-1}) and it has been reported that, the band at 3500 cm^{-1} is due to a hydrogen-bond-free OH^- groups, the band at 3000 cm^{-1} is due to weak hydrogen bonding between OH^- groups and NBO and the band at 2500 is due to the strongest hydrogen bonding of OH^- to NBO [31]. The OH^- groups are coupled to different environments with different coordination states species, mainly TeO_4 tbps,TeO_{3+1} units and TeO_3 tps (which are associated with NBO) of the glass matrix. In TeO_2-based glasses with modifiers, the OH^- groups are mainly hydrogen-bonded to the network former cations T^{4+} because of its large field strength and its high content [32]. The band at 2764 cm^{-1} is due to the fundamental stretching vibrations of the OH^- groups, which are strongly hydrogen-bonded (Te–O–OH–Te) to the TeO_4 tbps and to the TeO_{3+1} or the TeO_3 pyramids constituting the glass matrix [31].

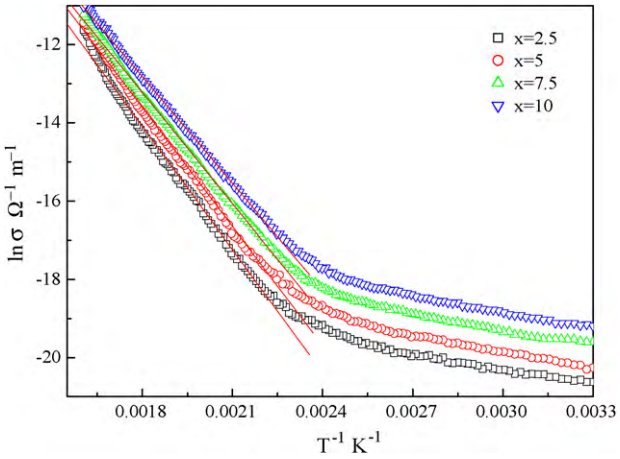

Fig. 5. Temperature dependence of dc conductivity ($\ln \sigma_{dc}$) for different glass compositions.

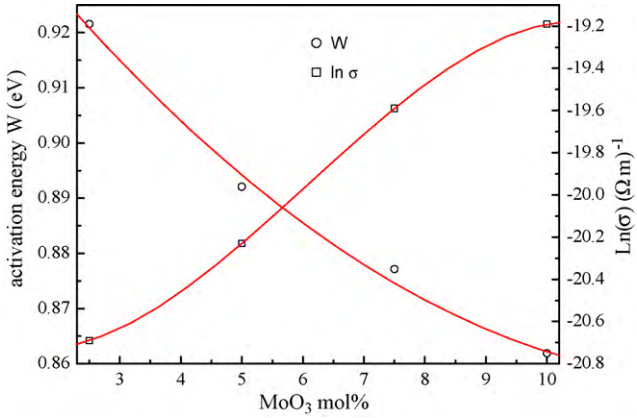

Fig. 6. Effect of MoO_3 content on dc conductivity ($\ln \sigma_{dc}$) at $T = 476$ K and activation energy (W) for different glass compositions.

The band at 3085 cm^{-1} is assigned to the stretching vibrations of the OH^- groups, which are weakly hydrogen-bonded to the glass matrix through the (Te–O–HO–Te) bridges [33]

As seen in Fig. 4, the intensity of the two Raman bands at 2964 and 3080 cm^{-1} is increasing and that for the bands at 2764 and 2869 cm^{-1} is decreasing as the MoO_3 content increased.

3.3. dc conductivity

The dependence of log rdc on the reciprocal temperature is shown in Fig. 5 for the $(75-x)TeO_2$–$15PbCl_2$–$xMoO_3$–$10ZrO_2$ doped with 5 mol% Er_2O_3, where $x = 2.5$, 5, 7.5 and 10 mol%, glass system. The slope of the curves which gives the activation energy for conduction W. The linear relationship between the logarithm of dc conductivity ($\ln \sigma$; σ is expressed in ($\Omega\,m^{-1}$)) and inverse of temperature with a negative slope indicates that the following well-known Arrhenius law is satisfied [34,35]:

$$\sigma = \sigma_o \exp\left(\frac{-W}{kT}\right) \quad (2)$$

where, σ_o is the pre-exponential factor, W is the activation energy, K is the Boltzmann constant and T is the temperature measured in Kelvins. From Fig. 5 it is observed that the dc conductivity in present glass system increase with rise in temperature. Also the dc conductivity is found to increase with increase in the concentration of MoO_3. The increase in electrical conductivity of the present glass system with increase MoO_3 content can be attributed to the increase molybdenum ions [36]. The effect of molybdenum content on the dc conductivity $\ln \sigma$ at $T = 476$ K and activation energy W for the present glass system shown in Fig. 6. It is evident from Fig. 6 that with increase in the concentration of MoO_3, can be observed that, the values of the conductivity to increase and the activation energy for dc conduction to decrease. The reasons for such changes may be due to gradual conversion of MoO_4^{2-} groups to $MoO^{5+}O_3^-$ complexes and MoO_6 groups in the glass network which act as modifiers. Also these modifier groups weaken the lead–tellurite glass network and create pathways suitable for migration of free ions that build up space charge. Thus, the build up space charge polarization result an increase in the dielectric parameters [37].

The activation energy W and enter atomic distance between molybdenum ions R are estimated and listed in Table 1, the activation energy W depends on the site-to-site distance R. These results show that there is a prominent positive correlation between the activation energy W and enter atomic distance between molybdenum ions R. This positive correlation is similar to that suggested in glasses containing transition metal ions [38,39]. The results in Table 1 indicate that as MoO_3 content increases, enter atomic distance between molybdenum ions R decreases. It is understood that this causes the activation energy for conduction W to decrease, while causing the dc conductivity σ to increase. The conductivity in the glasses studied can be assumed to be due to electronic hopping from the lower valence state Mo^{5+} (donor level) to the higher valence state Mo^{6+} (acceptor level). This conduction mechanism is similar to that proposed in other transition metal oxides [19,39]. The ionic conduction is expected due to the diffusion of $PbCl_2$ ions where chlorine behaves as alkali ions [16,17]. Therefore, the conductivity in the present glasses is electronic and ionic in nature.

3.4. Optical band gap

The optical transmittance spectra for the $(75-x)TeO_2$–$15PbCl_2$–$xMoO_3$–$10ZrO_2$ doped with 5 mol% Er_2O_3, where $x = 2.5$, 5, 7.5 and 10 mol%, glass system are shown in Fig. 7. The spectra of the glass samples with different concentrations of MoO_3 are similar except for the band intensities, which are dependent on the MoO_3 concentration. The observed peaks are assigned to the transitions from the $^4I_{15/2}$ ground state to the excited states of Er^{3+} ions. That is, the peaks at 425, 489, 521, 544, 652, 799, and 977 nm are corresponding to the $^4I_{15/2} \rightarrow {}^4F_{3/2} + {}^4F_{5/2}$, $^4I_{15/2} \rightarrow {}^4F_{7/2}$, $^4I_{15/2} \rightarrow {}^2H_{11/2}$, $^4I_{15/2} \rightarrow {}^4S_{3/2}$, $^4I_{15/2} \rightarrow {}^4F_{9/2}$, $^4I_{15/2} \rightarrow {}^4I_{9/2}$ and $^4I_{15/2} \rightarrow {}^4I_{11/2}$ transitions, respectively [40].

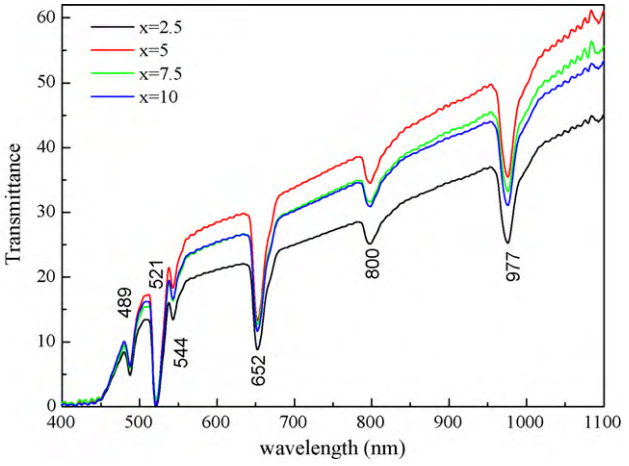

Fig. 7. The transmittance spectra for different glass composition.

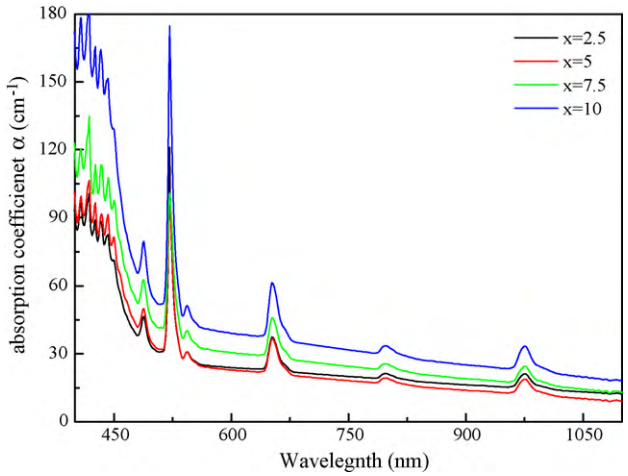

Fig. 8. The absorption coefficient as a function of wavelength for the glass system.

The optical absorption spectra for all the glass compositions are shown in Fig. 2 for wavelength region around absorption edge. The optical absorption coefficient, α, which is the relative rate of decrease in light intensity along its path of propagation, was calculated from the transmittance data in the wavelength range 190–1100 nm. Fig. 8 shows a plot of α as a function of phonon energy for the glass system. The optical absorption coefficient α for the glass samples was calculated using the relation [41]:

$$\alpha = \frac{1}{d}\ln\frac{I_o}{I_t} \tag{3}$$

where d is the thickness of the sample and I_o and I_t are the intensities of incident and transmitted radiations, respectively. The factor $\ln(I_o/I_t)$ is the transmittance, 'T'. For amorphous materials the optical absorption at higher value of $\alpha(\nu)$ ($\geq$104 cm^{-1}) above the exponential tail follows a power law given by Davis and Mott which in the most general form is given by [34]:

$$\alpha(\nu) = \frac{[B(h\nu - E_{opt})]^r}{h\nu} \tag{4}$$

The exponent r determines the type of electronic transitions causing the absorption and takes the values 1/2, 3/2, 2, and 3 for direct allowed, direct forbidden, indirect allowed and indirect forbidden transitions, respectively, B is a constant called band-tailing parameter, E_{opt} is the optical band gap energy and $h\nu$ is the incident photon energy. For amorphous materials, indirect transitions (r = 2 and 3) are valid according to the Tauc's relations [42]. The variation of $(\alpha h\nu)^{1/2}$ vs. $h\nu$ (Tauc's plot) is shown in Fig. 9 for the glass system. The values E_{opt} can be obtained (using Eq. (4)) by extrapolating the linear region of the curves in Fig. 9 for $(\alpha h\nu)^{1/2} = 0$ [42,43] and are given in Table 2.

From the analysis of optical transmittance spectra it is found that optical absorption edge is not sharply defined in the glass systems under study, which clearly indicates their amorphous nature. It is also observed from Fig. 8 that the fundamental absorption edge and cut-off wavelength ($\lambda_{cut\text{-}off}$) shift towards lower wavelength with increase in MoO_3 content in the glass systems. The decrease in

Table 2
Optical energy gap values E_{opt} obtained for indirect allowed and indirect forbidden transitions, and band tail energy E_r for the $(75-x)TeO_2$–$15PbCl_2$–$xMoO_3$–$10ZrO_2$ doped with 5 mol% Er_2O_3, where x = 2.5, 5, 7.5 and 10 mol% glass system.

Glass no.	E_{opt} (eV)p = 2	E_{opt} (eV)p = 1/3	E_{opt} (eV)
1	2.29	2.06	0.034
2	2.21	1.99	0.036
3	2.18	1.95	0.037
4	2.15	1.93	0.039

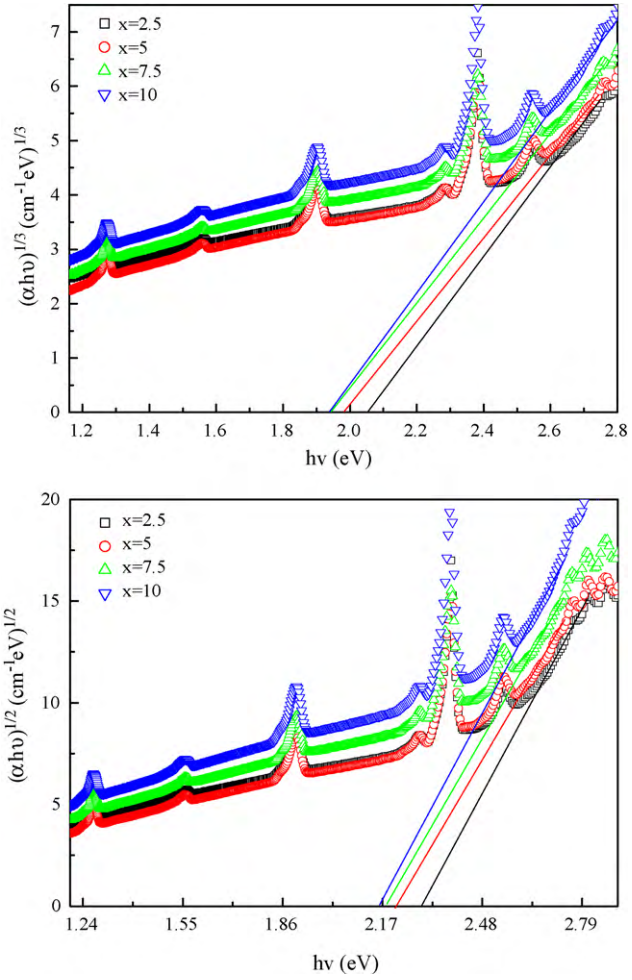

Fig. 9. The relation between photon energy eV and $(\alpha h\nu)^r$, where r = 2, and 3 for indirect allowed and indirect forbidden transitions, respectively for the glass system.

E_{opt} with increasing MoO_3 content for the glass system corresponds with the red shift in $\lambda_{cut\text{-}off}$. This suggests that the non-bridging oxygen (NBO) ions are increasing with the increasing concentration of MoO_3. For metal oxides (M–O), the valance band maximum VBM mainly consists of O(2p) orbital and the conduction band minimum CBM mainly consists of M(nS) orbital. The NBO ions contribute to VBM. When a metal–oxygen bond is broken, the bond energy is released and the non-bridging orbitals have higher energies than bonding orbitals [44]. Increase in concentration of NBO ions results in the shifting of VBM to higher energies and reduces the band gap.

The optical absorption and particularly the absorption band edge is a good method for studying optically induced transition and gives information about the structure and optical energy gap in glasses. The absorption edge in many materials follows the Urbach rule [45].

$$\alpha(h\nu) = \alpha_o \exp\left(\frac{h\nu}{E_r}\right) \tag{5}$$

where α is the optical absorption coefficient, α_o is a constant and (E_r) is the energy width of the tail of localized state in the normally forbidden band gap. E_r is often interpreted as the width of the localized states in the band gap of the material. The exponential dependence of the optical absorption coefficient with photon energy may arise from the electronic transitions between the localized states, which have tailed odd in the band gap. The density of these states falls off exponentially with energy, which is consistent with the theory of Tauc [46]. However, the exponential dependence

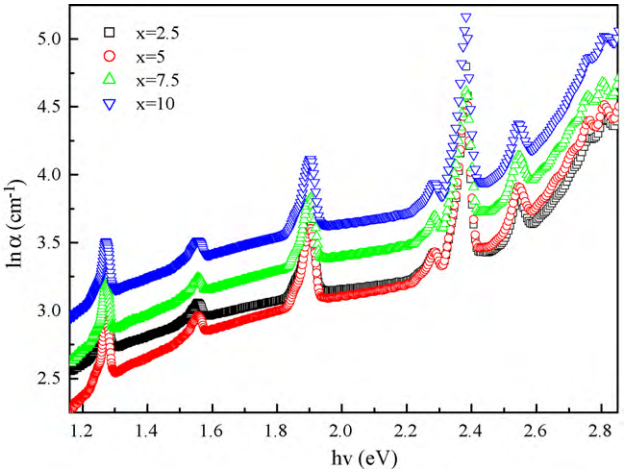

Fig. 10. The relation between $\ln \alpha\ cm^{-1}$ and photon energy eV for the glass system.

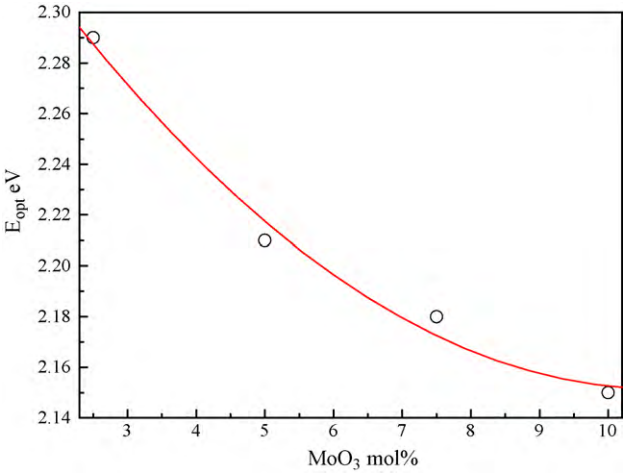

Fig. 11. The optical band gap E_{opt} as a function of MoO_3 content for the glass system.

of the optical absorption coefficient on energy might arise from the random fluctuations of the internal fields associated with the structural disorder in many materials. The width of the localized states (band tail energy or Urbach energy) E_r is estimated from the slopes of $\ln(\alpha)$ vs. $h\nu$ plots. Fig. 10 shows the variation of $\ln \alpha$ with incident photon energy $h\nu$ for the glass system. As seen in the figure, the absorption edge is found to be exponentially dependent on the incident photon energy and obeys the empirical Urbach rule [45]. The width of the localized states E_r (band tail energy or Urbach energy) estimated from the slopes of $\ln \alpha$ vs. $h\nu$ plots was found to be in the range 0.034–0.039 eV. A plot of E_{opt} for indirect allowed transition against MoO_3 content shows that E_{opt} decreases with an increase in MoO_3 content as shown in Fig. 11. The decreasing values of E_{opt} can be attributed to the structural changes that are taking place in the studied glass system and increase of non-bridging oxygen (NBO) ions.

4. Conclusions

Homogeneous glasses can be prepared in the series $(75-x)TeO_2$–$15PbCl_2$–$xMoO_3$–$10ZrO_2$ doped with 5 mol% Er_2O_3, where $x = 2.5$, 5, 7.5 and 10 mol%. Structural studies by Raman spectroscopy revealed MoO_4 and MoO_6 as basic structural units formed by molybdenum atoms in these glasses. The ratio of MoO_6/MoO_4 increases with increasing content of MoO_3 in these glasses, as reflected in the Raman spectra. The incorporation of molybdate units into the tellurite glasses, structural network results in the progressive formation of distorted TeO_{3+1} units followed by the creation of trigonal TeO_3 pyramids (tps) associated with non-bridging oxygen atoms (NBO), besides the formation of Te–O–Mo bonds. The dc conductivity increases with increase in MoO_3 content, this increase can be attributed to the increase of molybdenum ions. The activation energy decreases with increase in MoO_3 content. The electrical conduction in present glass system is ionic and electronic in nature. From the present study, it is observed that the optical band gap decreases with increase in MoO_3 content due to an increase in the concentration of non-bridging oxygens. The optical band gap obtained for indirect allowed and indirect forbidden transitions, and the present glasses behave as indirect gap semiconductors. Because of structural changes in the glass network the density decreases with increase in MoO_3 content. The variation in molar volume with MoO_3 content indicates that the effect of MoO_3 on the glass structure is dependent on its concentration.

References

[1] Y. Gandhi, N. Venkatramaiah, V. RaviKumar, N. Veeraiah, J. Physica B 404 (2009) 1450–1464.
[2] L.R.P. Kassab, R.de.A. Pinto, R.A. Kobayashi, M. Piasecki, P. Bragiel, I.V. Kityk, J. Opt. Commun. 281 (2008) 3721.
[3] D. Tatar, M.L. Ovecoglu, G. Ozen, J. Eur. Ceram. Soc. 28 (2008) 3097.
[4] A. Mekki, G.D. Khattak, L.E. Wenger, J. Non-Cryst. Solids 351 (2005) 2493–2500.
[5] D.K. Durga, N. Veeraiah, Physica B 324 (2002) 127.
[6] M.A. Villegas, J.M. Fernandez Navarro, J. Eur. Ceram. Soc. 27 (2007) 2715–2723.
[7] M. Prasanth Kumar, T. Sankarappa, Solid State Ionics 178 (2008) 1719.
[8] S. Rada, M. Culea, E. Culea, J. Non-Cryst. Solids 354 (2008) 5491–5495.
[9] E.S. Yousef, M. Hotzel, C. Russel, J. Non-Cryst. Solids 354 (2008) 4675.
[10] S. Sakida, S. Hayakawa, T. Yoko, J. Non-Cryst. Solids 243 (1999) 13–25.
[11] A.H. Khafagy, A.A. El-Adawy, A.A. Higazy, S. El-Rabaie, A.S. Eid, J. Non-Cryst. Solids 354 (2008) 1460–1466.
[12] M.R. Sahar, K. Sulhadi, M.S. Rohani, J. Non-Cryst. Solids 354 (2008) 1179–1181.
[13] H.T. Sun, S.X. Dai, S.Q. Xu, Physica B 352 (2004) 366–371.
[14] H. Nasu, O. Matsushita, K. Kamiya, H. Kubodera, J. Non-Cryst. Solids 124 (1990) 275.
[15] I.V. Kityk, J. Kasperczyk, K. Plucinski, J. Opt. Soc. Am. B 16 (10) (1999) 1719.
[16] A. Hall, J. Swenson, S. Adams, C. Meneghini, Phys. Rev. Lett. 101 (2008) 195901.
[17] S.S. Das, N.B. Singh, J. Mater. Res. Bull. 43 (2008) 3008.
[18] L. Srinivasa Rao, M. Srinivasa Reddy, D. Krishna Rao, N. Veeraiah, J. Solid State Sci. 11 (2009) 578.
[19] L. Bih, M. El Omari, J.M. Reau, A. Nadiri, A. Yacoubi, M. Haddad, J. Mater. Lett. 50 (2001) 308–317.
[20] A.E. Miller, K. Nassau, K.B. Lyons, M.E. Lines, J. Non-Cryst. Solids 99 (1988) 289.
[21] B.V.R. Chowdari, P. Pramoda Kumari, J. Phys. Chem. Solids 3 (58) (1997) 515.
[22] J.W. Kantelhardt, St. Russ, A. Bunde, Phys. Rev. B 63 (2001) 064302.
[23] C. Duverger, M. Bouazaoui, S. Turrell, J. Non-Cryst. Solids 220 (1997) 169.
[24] A. Jha, S. Shen, M. Naftaly, Phys. Rev. B 62-10 (2000) 6215.
[25] M. Udovic, P. Thomas, A. Mirgorodsky, O. Durand, M. Soulis, O. Masson, T. Merle-Me jean, J.C. Champarnaud-Mesjard, J Solid State Chem. 179 (2006) 3252–3259.
[26] I. Shaltout, Y. Badr, J. Physica B 381 (2006) 187–193.
[27] M. Arnudov, Y. Dimitriev, V. Dimitrov, M. Dimitrova-Pankova, Phys. Chem. Glasses 27–1 (1986) 48.
[28] T. Sekiya, N. Mochida, S. Ogawa, J. Non-Cryst. Solids 185 (1995) 135–144.
[29] A. Berthereau, Y.LE. Luyer, R. Olazcuaga, Mater. Res. Bull. 29 (1994) 933.
[30] V.O. Sokolov, V.G. Plotnichenko, V.V. Koltashev, I.A. Grishin, J. Non-Cryst. Solids 355 (2009) 239–251.
[31] V. Nazabal, S. Todoroki, A. Nukui, T. Matsumoto, S. Suehara, T. Hondo, T. Araki, S. Inoue, C. Rivero, T. Cardinal, J. Non-Cryst. Solids 325 (2003) 85–102.
[32] X. Feng, S. Tanabe, T. Hanada, J. Non-Cryst. Solids 281 (2001) 48.
[33] G. Amarnath, S. Buddhudu, F.G. Brayant, J. Lumin. 15 (1991) 17.
[34] N.F. Mott, E.A. Davis, Electronic Processes in Non-Crystalline Materials, 2nd ed., Clarendon Press, Oxford, 1979.
[35] N.F. Mott, Metal Insulator Transitions, Taylor & Francis, London, 1974.
[36] P.S. Gahlot, A. Agarwal, V.P. Seth, S. Sanghi, S.K. Gupta, M. Arora, Spectrochim. Acta Part A 61 (2005) 1189–1194.
[37] P. Syam Prasad, B.V. Raghavaiah, R. Balaji Rao, C. Laxmikanth, N. Veeraiah, J. Solid State Commun. 132 (2004) 235–240.
[38] M. Sayer, A. Manshingh, Phys. Rev. B 6 (1972) 4629.
[39] M. Shaaban, Salem, J. Mater. Sci. 44 (2009) 5760–5767.
[40] H.-W Li, S.-Q. Man, J. Opt. Commun. 282 (2009) 1579–1583.
[41] E.A. Davis, N.F. Mott, Philos. Mag. 22 (1970) 903.
[42] J. Tauc, Amorphous and Liquid Semiconductor, Plenum Press, New York, 1974.
[43] Y. Moustafa, A. Hassan, G. El-Damrawi, N. Yevtushenko, J. Non-Cryst. Solids 194 (1996) 34.
[44] R. Jose, T. Suzuki, Y. Ohishi, J. Non-Cryst. Solids 352 (2006) 5564.
[45] F. Urbach, Phys. Rev. 92 (1953) 1324.
[46] J. Tauc, Amorphous and Liquid Semiconductor, Plenum, New York, 1974.